Applied Catalysis B: Environmental 237 (2018) 613–621

Contents lists available at ScienceDirect

Applied Catalysis B: Environmental

journal homepage: www.elsevier.com/locate/apcatb

H-doped TiO_{2-x} prepared with MgH_2 for highly efficient solar-driven hydrogen production

Apurba Sinhamahapatra[a,1], Ha-Young Lee[a], Shaohua Shen[b], Samuel S. Mao[c,*], Jong-Sung Yu[a,*]

[a] Department of Energy Science and Engineering, DaeguGyeongbuk Institute of Science and Technology (DGIST), Daegu, 42988, Republic of Korea
[b] International Research Center for Renewable Energy, State Key Laboratory of Multiphase Flow in Power Engineering, Xi'an Jiaotong University, Shaanxi 710049, China
[c] Department of Mechanical Engineering, University of California at Berkeley, Berkeley, CA 94720, USA

ARTICLE INFO

Keywords:
Photocatalysis
Visible light
Solar hydrogen
Reduced TiO_2

ABSTRACT

Efficient utilization of visible light with high stability remains a critical challenge for solar-driven photochemical generation of hydrogen (H_2) using particulate photocatalysts. Black TiO_2 was introduced with remarkable enhancement of visible light absorption, but its efficiency in the visible light has not reached the desired level for real-world applications. Here we report a gold-colored H-doped TiO_{2-x} (H:TiO_{2-x}) nanoparticles prepared by controlled reduction via simultaneous presence of [Mg] and [H], which are obtained from the decomposition of MgH_2. The H-doped TiO_{2-x} exhibits a significant activity (16.1 $mmol g^{-1}h^{-1}$) and remarkable stability after Pt deposition for solar-driven H_2 generation from methanol-water. The excellent photoactivity of H-doped TiO_2 can be attributed to oxygen vacancies and H doping at the reduced TiO_{2-x} surface generated by [Mg] and [H]. The H-doped TiO_2 is also producing H_2 from methanol-seawater with a rate of 6.1 $mmol g^{-1}h^{-1}$ under simulated sunlight.

1. Introduction

Alternate energy resources are the prime concern of the present generation, and hydrogen (H_2) is one of the cleanest energy carriers as it produces only water as the main product upon oxidation [1–3]. Sunlight-induced H_2 production from water is one of the most desired solutions to this issue [4–6]. Among different approaches to sunlight-induced H_2 production from water, direct photochemical (PC) water splitting is the simplest and most practical compared to photovoltaic electrolysis (PVE) and photoelectrochemical (PEC) water splitting [7]. However, the utilization of sunlight is not as straight as the main usable part of the sunlight is visible (VIS) light (~46%), and there is a lack of photocatalyst system working efficiently for visible light-assisted photochemical hydrogen production. In this concern, the development of efficient photocatalyst system for sunlight-induced photochemical hydrogen production is one of the most challenging tasks in the present times.

TiO_2 is one of the most active and most studied photocatalysts for ultraviolet (UV) light-induced H_2 production [2,8–10]. Among the numerous approaches that were studied to modify TiO_2 for visible light-assisted H_2 production, development of black TiO_{2-x} in recent past is one of the most encouraging findings [6,11–27]. Black or reduced TiO_{2-x} showed dramatic increment in the light absorption in the visible and infrared (IR) region along with the UV light. However, the visible light activity for hydrogen production fails to accomplish the expectation. Despite this, there is a huge increment in UV light activity compared to the corresponding white TiO_2 [28]. Although the amount of UV light is small in sunlight, the overall sunlight activity of reduced black TiO_{2-x} was promising and thus stimulated further research on the improvement of the materials. Different black TiO_{2-x} materials with different fabrication methods have been reported, which resulted in improvement of visible light activity for H_2 production as well as overall sunlight activity that creates further hope. Therefore, it desires further investigation [13,17].

In this report, we present our recent findings on outstanding sunlight-induced H_2 production performance of platinized H-doped reduced TiO_{2-x} (H:TiO_{2-x}). We demonstrate a control reduction of commercial (Aldrich) nano-anatase TiO_2 by in-situ produced dual reducing agents ([Mg] and [H]) obtained from MgH_2 decomposition at 500 °C in Ar atmosphere for the first time. Previously, different metal hydrides like CaH_2, $NaBH_4$, NaH, were used to prepare reduced or black TiO_2 [12,14–17,21,29–31]. Most of the metal hydrides were used to release active hydrogen as a promising reductant [17]. Tominaka et al [12]. used a fourfold molar excess of CaH_2 powder to prepare black TiO_2 at

* Corresponding authors.
E-mail addresses: ssmao@lbl.gov (S.S. Mao), jsy119@gmail.com (J.-S. Yu).
[1] Present affiliation: Department of Chemical Engineering, Indian Institute of Technology (ISM), Dhanbad, 826004, Jharkhand, India.

https://doi.org/10.1016/j.apcatb.2018.06.030
Received 4 April 2018; Received in revised form 2 June 2018; Accepted 11 June 2018
Available online 15 June 2018
0926-3373/

350 °C for 15 days. Later on, Zhu et al [21]. prepared black TiO_2 with a crystalline core–amorphous shell structure reduced by CaH_2 at 400 °C, which exhibited 1.7 times higher H_2 production than the pristine white TiO_2. $NaBH_4$ was also used extensively for the preparation of reduced TiO_2 by different approaches like dry method, wet method, and sol-gel method [15,15,16,17,30–34]. Most of the study explains that the release of active hydrogen from $NaBH_4$ is responsible for reduction, which creates oxygen vacancies and increases the photocatalytic activity. Another, interesting metal hydride is TiH_2, which is also used as a reducing agent although it is used as a source of TiO_2 [35,36]. Zhu et al. produced hydrogenated blue titania by using TiH_2 as a reducing agent from P25 [36]. The prepared photocatalyst showed almost double photocatalytic activity than that of pristine P25. However, the concept of dual reducing agents from metal hydride was not realized earlier for the preparation of black or reduced TiO_2 although metal hydrides were used [12,13,16,17,36].

Recently, we have found that controlled magnesiothermic reduction of metal oxides in the presence of molecular H_2 (5% H_2/Ar) produced reduced metal oxides with enhanced solar light absorbance and improved photo-assisted H_2 production ability [37,38]. It was observed that the high activity of TiO_{2-x} [37] was achieved only when both Mg and H_2 were used in reducing conditions. This suggests that the simultaneous presence of two different reducing species generates more efficient photocatalyst, which creates quires of what would be the effect of the simultaneous presence of active [Mg] and [H] produced at the same time in a confined microenvironment on TiO_2 surface. However, in the case of the magnesiothermic reduction in the presence of H_2, the active reducing species [Mg] and [H] are generated from the different origins such as bulk Mg metal and molecular H_2 and result in inhomogeneous distribution of the active species. To study the above hypothesis, we have chosen MgH_2 as it can offer fresh formation of active reducing species i.e. [Mg] and [H] at the same time on thermal decomposition. Also, the magnesiothermic reduction needed higher temperature (650 °C) due to high melting point of Mg, which resulted in phase impurity and low surface area. In current work, we have performed the experiment at 500 °C as decomposition of MgH_2 can be obtained at lower temperature (327 °C) [39]. MgH_2 is also quite stable in handling at ambient conditions unlike some other metal hydrides such as CaH_2 and NaH, which need special caution in handling [12,14,21].

2. Experimental methods

2.1. Preparation of H-doped TiO_{2-x} ($H:TiO_{2-x}$)

In a typical experiment, 4 g of commercial white anatase TiO_2 nanoparticles (Sigma-Aldrich) is well mixed with the desired amount of MgH_2 (Alfa Aesar) and heated in Ar atmosphere at 500 °C for 8 h in a tube furnace. The obtained material was subjected to stirring in dilute HCl for 1 day to remove Mg species, and washed with water and ethanol. The washed material was collected, dried in the oven at 80 °C. Different molar ratios (x = 0.3, 0.5, 0.75, and 1) of MgH_2 with respect to TiO_2 were used to produce different colored reduced samples and named as RT-MH-x (where, x = 0.3, 0.5, 0.75, and 1). The materials were characterized with different techniques and used for the further experiment. For comparison, related reduced TiO_{2-x} samples were also prepared using H_2/Ar, Mg/Ar, and Mg/H_2/Ar. In the case of using Mg/Ar or Mg/H_2/Ar, the samples were heated at 650 °C for 8 h instead of 500 °C since metallic Mg starts to melt around at 600 °C and higher. As mentioned above, the reduction temperature is set at 500 °C unless otherwise specifically mentioned.

2.2. Characterization

Powder X-ray diffraction (XRD) pattern of the samples was recorded using a Rigaku Smartlab diffractometer with Cu-Kα (λ = 0.15406 nm) operated at 40 kV and 30 mA at a scan rate of 4° min^{-1}. Raman spectra of the samples were obtained from a Raman spectrometer (NICOLET ALMECA XR, Thermo Scientific) using 532 nm laser beam for excitation. High-resolution transmission electron microscopy (HR-TEM) and high-resolution scanning electron microscope (HR-SEM) images were collected using JEOL FE-2010, operated at 300 kV. Ultraviolet-visible-near infrared diffuse reflectance spectra (UV-VIS-NIR DRS) of the samples were recorded by using a UV-VIS-NIR spectrophotometer (CARY 5000, Agilent Technologies). X-ray photoelectron spectroscopy (XPS) spectra were collected using an ESCALAB 250 XPS System with a monochromated Al Kα (150 W) source. Photoluminescence spectra were obtained from a Cary Eclipse Fluorescence Spectrophotometer (Agilent Technologies). Solid-state magic angle spin (MAS) nuclear magnetic resonance (NMR) spectra were acquired from a 600 MHz Solid-state NMR (14.1 T) spectrometer (Unity INOVA, Agilent Technologies, U.S.A). Nitrogen adsorption–desorption isotherms were measured at −196 °C using a Micromeritics ASAP 2460 accelerated surface area and porosity analyzer after the samples were degassed at 150 °C to 20 mTorr for 12 h. The specific surface area was determined based on Brunauer–Emmett–Teller (BET) method from nitrogen adsorption data in the relative pressure range from 0.05 to 0.2. ICP-OES analyses using iCAP7400 (Thermo Scientific) were carried out to know the Pt loading amount. Each of Pt-loaded samples was added to 10 ml of aqua regia and the Pt solution was diluted 10 times by water before the ICP analysis.

2.3. Photo-Deposition of Pt nanoparticles and H_2 production

Photocatalytic reactions were performed in a cylindrical quartz reactor under continuous Ar flow with a fixed rate using a projected side-face light beam. The maximum illuminated area was 15.75 cm^2 considering the cross-section of the cylindrical reactor containing 50 ml of solution. The produced H_2 was carried directly to a connected GC (Bruker 450) by Ar flow and determined by TCD detector. In a typical experiment, 20 mg of catalyst was dispersed in 20% 50 ml of methanol-water, and the desired amount of aqueous solution of H_2PtCl_6 was added. The solution was subjected to light obtained by a 450 W Xe light source embedded with liquid IR filter for 2 h. Pt nanoparticles were photo-deposited with around 2–3 nm in size and nicely distributed on titania surface (Fig. S11). After Pt loading, the same solution was studied for H_2 generation under simulated sunlight (1 Sun, AM 1.5 G) obtained from a solar simulator.

Pt-loading amount on RT-MH-0.5 samples was determined by ICP-OES analysis 0.11, 0.24. 0.49, and 0.96 wt% Pt loadings, which were termed 0.1. 0.25, 0.5, and 1 wt % Pt-loaded RT-MH-0.5, respectively.

2.4. Performance stability of the developed photocatalyst for H_2 production under simulated sunlight

The performance stability of the developed Pt-loaded H-doped TiO_{2-x} photocatalyst was studied by identical reaction conditions as mentioned in the Experimental Section 2.3. 0.25% Pt-loaded RT-MH-0.5 was studied in two different sets of experiments. In the first set of the experiment, the reaction was run for continuous 50 h, and the 5 ml of methanol was added as H_2 production rate was slightly decreased, and the reaction was run again for another 50 h. In another set of experiment, the reaction was run for 4 h per day and continued for 25 days, and then the tested sample was stored in a closed dark bottle for 25 days and run again in the same way for another 25 days, *i.e.,* a total of 200 h (50 run) of run in 75 days. Before every run, the 50 ml volume of the reaction solution was checked, and methanol was added if necessary to make up.

2.5. H_2 production from seawater under simulated sunlight

As seawater is the largest natural source of water on earth, the

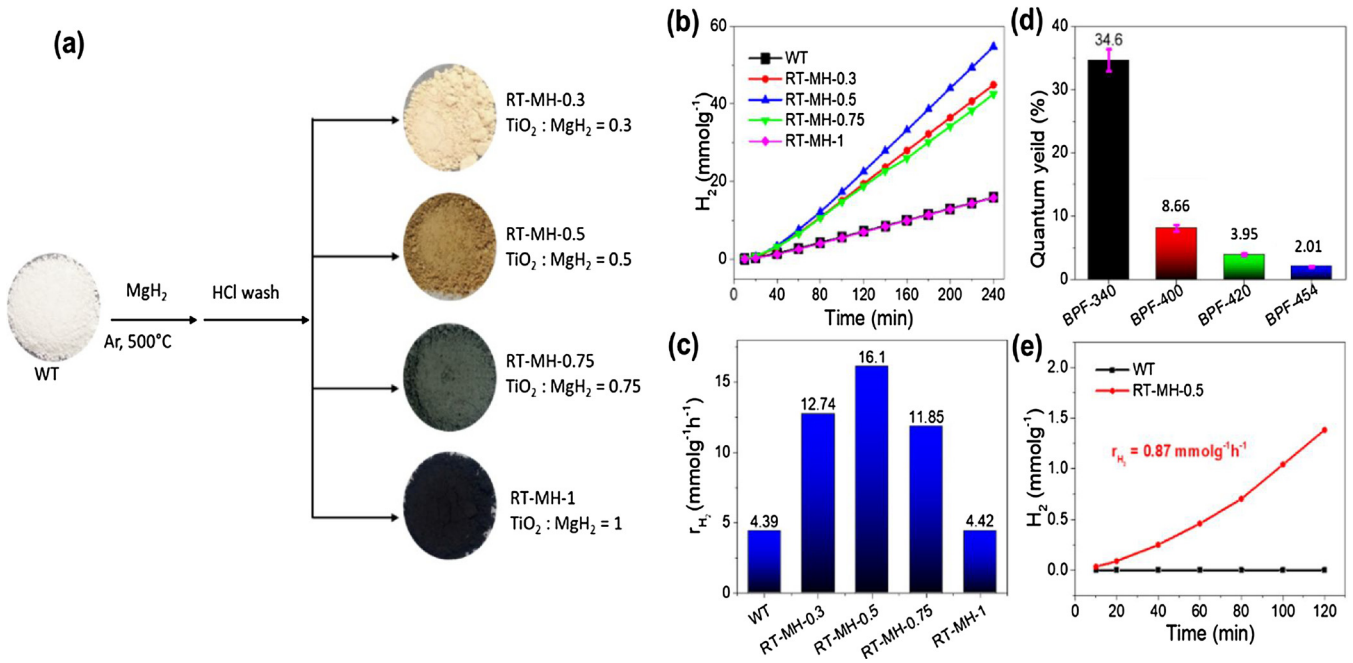

Fig. 1. Synthesis and hydrogen production. (a) Schematic representation of the synthesis of reduced TiO_2 with corresponding color (photograph). (b) Continuous H_2 generation profiles and (c) rate of H_2 generation in the presence of 1% Pt as a co-catalyst from methanol-water under simulated sunlight (AM 1.5 G, 1 Sun) for different samples. (d) Quantum yields for the corresponding wavelengths and e, visible light-assisted H_2 production from methanol-water using RT-MH-0.5 and Pt as co-catalyst. Visible light was obtained by using a cut-on filter in the wavelength range of 395 to 780 nm.

developed photocatalyst system was validated using seawater instead of pure deionized water. In a typical procedure, collected seawater (pH ~8.5) was filtered using Whatman filter paper (grade 2) before use for hydrogen production in the presence of methanol as a sacrificial reagent. The platinized RT-MH-0.5 was dispersed in seawater, and the photochemical reaction was performed as mentioned in the Experimental section 2.3.

3. Results and discussion

Different molar ratios of MgH_2 (x) and commercial white TiO_2 (WT) were used to produce different reduced samples (RT-MH-x, x = 0.3, 0.5, 0.75, and 1) with different color from white to yellow, gray, and black respect to MgH_2 amount (Fig. 1a). The different color is indicating the different extent of light absorbance as well as the extent of reduction. First, the prepared samples were studied for the H_2 production from methanol-water in the presence of Pt as a co-catalyst under simulated sunlight (Fig. 1b and c). The golden yellow RT-MH-0.5 sample exhibited the maximum rate (r_{H_2}) of 16.1 $mmolg^{-1}h^{-1}$ which is ~ 3.6 times higher than that of WT (4.39 $mmolg^{-1}h^{-1}$) used in this study. The other samples also generated H_2 with a higher rate. As Pt was used as a co-catalyst, the amount of Pt was optimized and 0.25 wt% (weight percent) with respect to TiO_2 was found to be the minimum Pt amount to get the maximum activity for hydrogen production (Fig. S1). The observed quantum yield (QY) was 34.6% at 340 ± 10 nm, 8.66% at 400 ± 10 nm 3.95% at 420 ± 10 nm and 2.01% at 454 ± 10 nm (Fig. 1d and Fig. S2), and further confirm noticeable contribution of visible light in the total H_2 production. This indicates the enormous enhancement in overall activity (including activity using UV and VIS light) after reduction. Previously, it was found that the UV light activity was fascinatingly increased in black or reduced TiO_2 compared to its pristine white TiO_2 due to increased donor density provided by oxygen vacancies formed in reduced samples [13,17,28]. To confirm, RT-MH-0.5 was studied further for only visible light-induced hydrogen production using a cut-on filter. WT shows no activity in the visible light (Fig. 1e), whereas the RT-MH-0.5 shows outstanding r_{H_2} of 0.87 $mmolg^{-1}h^{-1}$ (Fig. 1e) which is almost 2 times higher than that of the reduced TiO_{2-x} prepared by magnesiothermic reduction in presence of H_2/Ar (Table S1) [37]. The r_{H_2} value also outperforms the previously reported activity obtained from other reduced TiO_{2-x} prepared by different methods. Here it should be noted that the activity of RT-MH-1 (Fig. 1c) was quite low compared to RT-MH-0.5 although the former shows black color and higher absorbance of VIS-IR light.

The samples were characterized by different techniques to understand the improved activities. XRD and Raman spectra were used to monitor the change in crystal structure induced by MgH_2 treatment. The XRD patterns (Fig. 2a) of all the reduced samples except RT-MH-1 indicate an anatase phase (JCPDS no. 21-1272), with a peak shifting towards the higher 2θ (Fig. 2b). Along with the peak shifting, the peak broadening is also observed as FWHM (Full width at half maxima) of the main anatase peak (2θ = 25.2°) is increased in reduced sample (Fig. 2b). These observations indicate the decrease of the interplanar distance of the crystalline phase [17], and a slight reduction in crystallite size due to lattice disorder induced by oxygen vacancies [19,40]. For RT-MH-1 (Figs. 2a and S3), the formation of TiO with cubic crystal system are observed during the reduction in the presence of high amount of MgH_2, suggesting that during reduction with up to the certain amount (< 1 mol ratio) of MgH_2, the crystal structure of anatase TiO_2 remains unaltered.

Furthermore, the reduced samples were characterized by Raman spectroscopy. In comparison to WT, the Raman signals observed for reduced samples show a clear (Fig. 2c and d) peak shifting (from 143.1 to 147.3 cm^{-1}) and broadening, which suggest the presence of oxygen vacancies [41]. The changes in Raman signals were also previously observed for black or reduce TiO_2 and attributed to the defects regarding oxygen vacancies or lattice disorder [17,42]. The phenomenon can be understood as the surface TiO_6 octahedral symmetry is destroyed via reduction of Ti^{4+} and removal of oxygen during reduction, which agrees with the XRD results. Raman spectrum of RTMH-1 (Fig. S4) exhibits entirely new peaks like XRD signals, which confirm the prominent change in material from anatase TiO_2 to TiO.

Ti 2p XPS spectra (Fig. 2e) of all the samples show the peaks of Ti^{4+} i.e. $2p_{3/2}$ and $2p_{1/2}$ at 458.6 and 464.0 eV, respectively [17]. A noticeable peak-shifting towards the lower binding energy of the Ti 2p

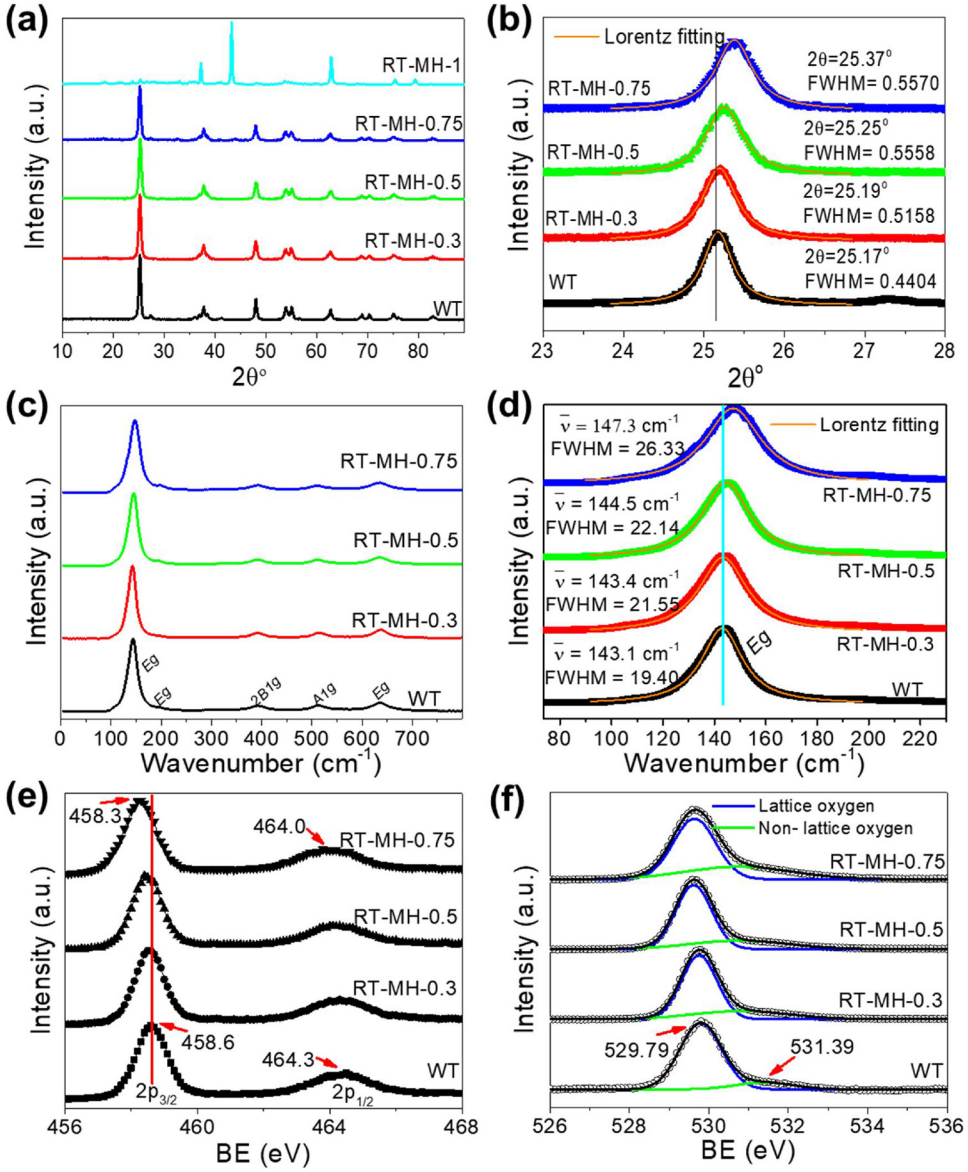

Fig. 2. Structural analysis, Ti^{3+} and oxygen vacancies. (a) Powder XRD patterns, (b) enlarged peak of 2θ = ~25.2, (c) Raman spectra and (d) enlarged strongest E_g peak of the different samples. High-resolution (e) Ti 2p and (f) O 1s XPS spectra of different samples.

peaks indicates the presence of Ti^{3+} in the reduced samples [17,43]. The amount of Ti^{3+} increases with the amount of MgH_2 used, probably due to more reduction. In the O 1 s XPS spectra (Fig. 2f), the signal for non-lattice oxygen corresponds mainly to surface hydroxyl groups [44]. Moreover, the relative % of non-lattice oxygen was increased with the amount of MgH_2 (Table S2), indicating the increment of oxygen vacancy in the reduced samples as the oxygen vacancy at surface transform to hydroxyl groups via reaction with water in air [44]. Furthermore, Mg 1 s XPS spectra (Fig. S5) confirm the absence of Mg in the final sample after HCl wash.

High resolution-transmission and scanning electron microscopic (HR-TEM and HR-SEM) analyses were further used to visualize the defects. The HR-TEM images (Figs. 3 and S6) of WT and RT-MH-0.5 show random defects on the particle, but the extent of defects is sufficiently increased for RT-MH-0.5. The corresponding line spectra (Fig. 3b and d) are further evidencing the lattice disorder in the defected area which satisfies the peak shifting and broadening in XRD and Raman spectra (Fig. 2a–d). Further, the FFT image (inset of Fig. 3a and c) corresponding to the RT-MH-0.5 is blurred compared to that of WT, which can also be attributed to presence of surface disorder [45]. The corresponding selected area electron diffraction (SAED) patterns (Fig. S6c) of both the samples indicate the different planes of anatase TiO_2 in agreement with XRD pattern. The obtained HR-SEM images (Fig. S7) also displayed more hollow area on surface of RT-MH-0.5 compared to that of WT.

The diffuse reflectance spectra (DRS) show an enhancement of absorption in the reduced samples compared to WT (Fig. 3e) in accordance with their color. Although the absorption is enhanced with the increase of MgH_2 amount, the absorption patterns of the different samples are not identical (Fig. 3e). The yellowish RT-MH-0.3 and H-doped RT-MH-0.5 show a sharp absorption peak at around 400 nm like WT and an additional formation of a new slope towards visible light up to < 700 nm, which justifies the yellow or golden color, but they do not show any absorption in IR region. The result indicates the formation of new shallow band states towards Fermi level to decrease the band gap. On the other hand, RT-MH-0.75 shows a continuously enhanced absorption in visible and IR light in addition to the sharp absorption at around 400 nm, and RT-MH-1 shows a continuous absorption of light in the full UV-VIS-IR region, justifying its black color. The band gap of the materials was calculated from Tauc plot (Fig. 3f). The WT shows a band

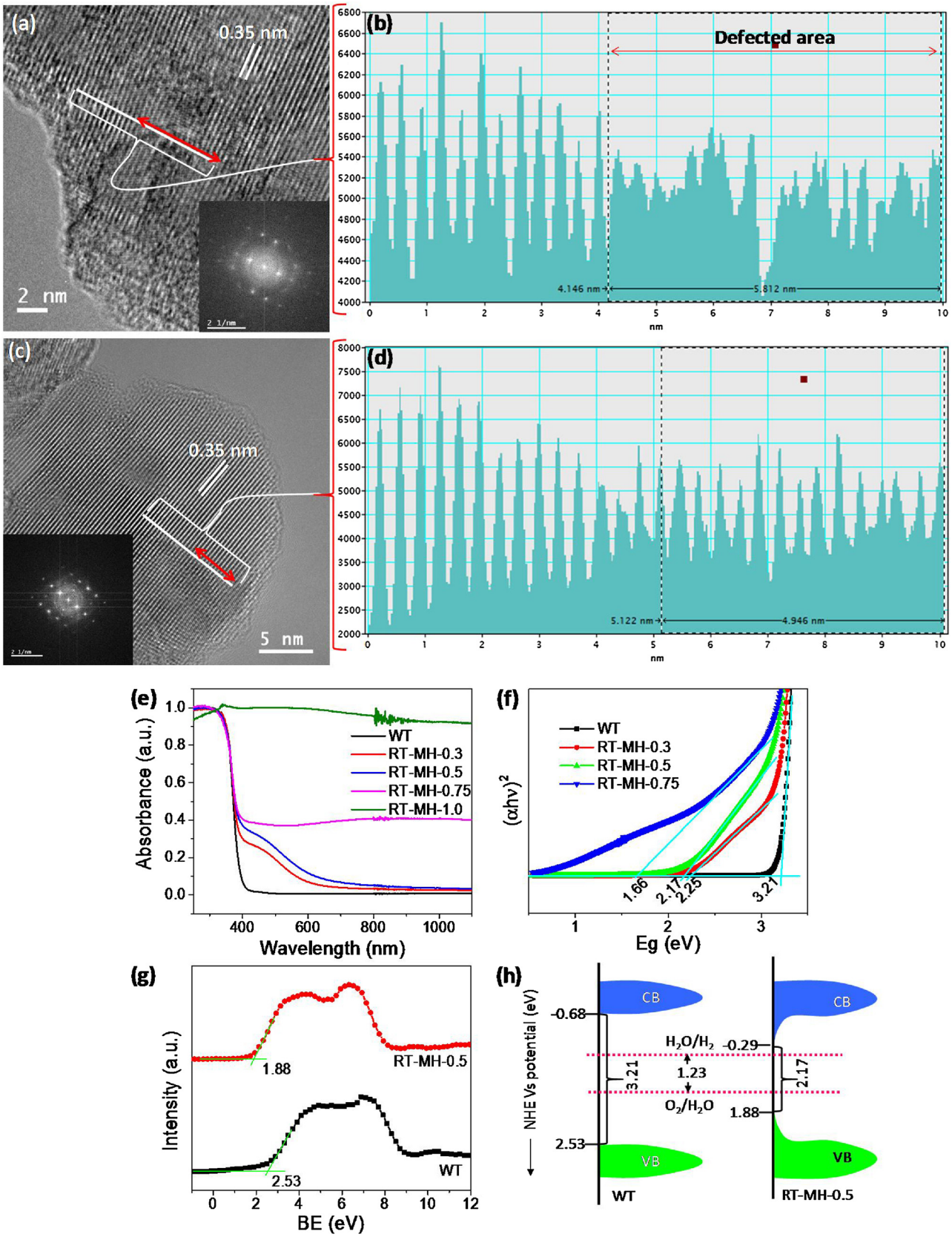

Fig. 3. Defects, Optical properties, and band structure. (a–b) HR-TEM image of RT-MH-0.5 (inset is corresponding FFT) with line profile of the selected area and (c–d) HR-TEM image of WT (inset is corresponding FFT) with line profile of the selected area. (e) Diffuse reflectance spectra (DRS) and (f) corresponding Tauc plots for different samples obtained from the absorption spectra. (g) Valence band XPS spectra of WT and RT-MH-0.5. (h) Probable band energy diagram (calculated from band gap and VB edge position) of WT and RT-MH-0.5 (the scales are arbitrary in the diagram).

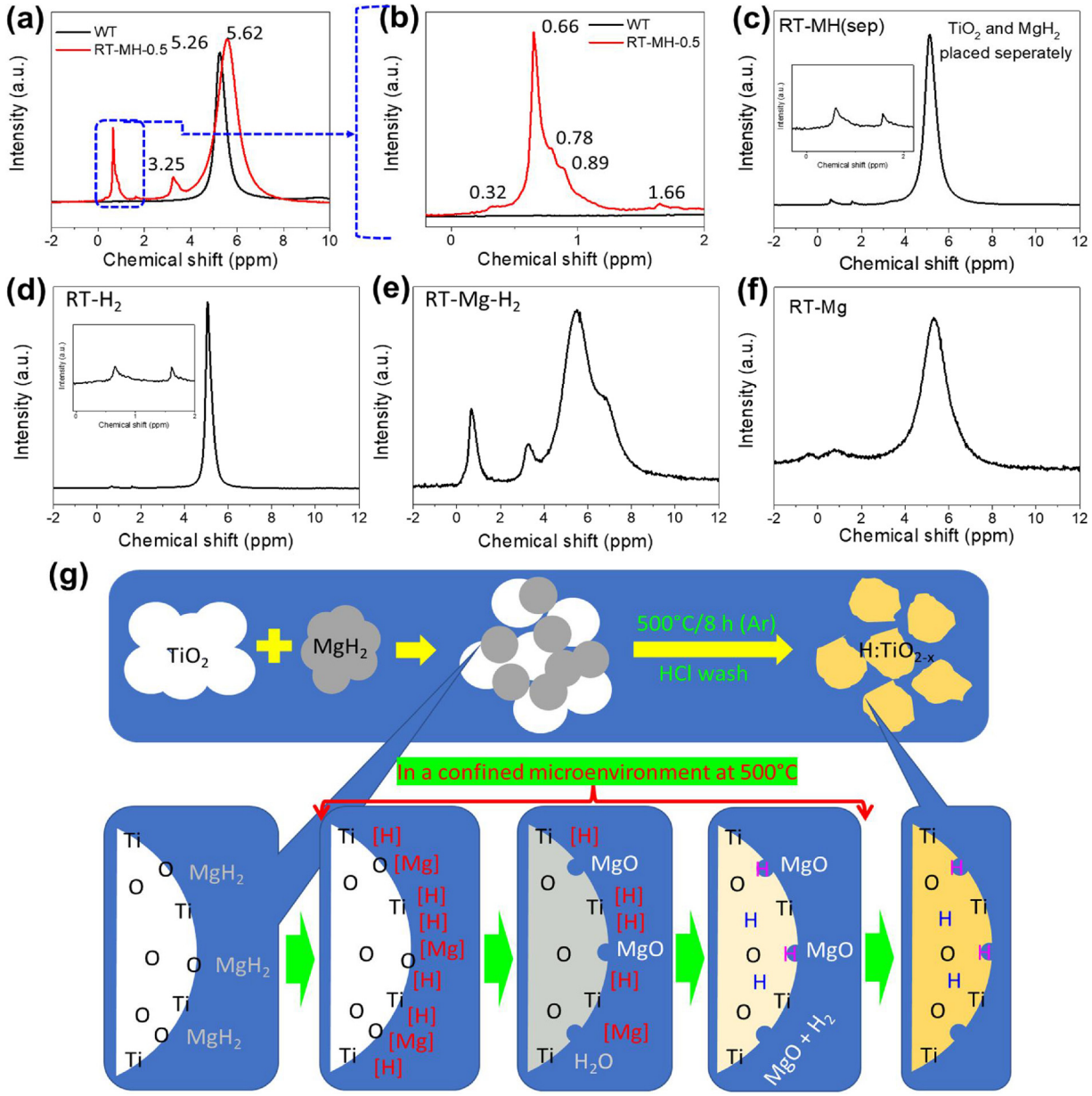

Fig. 4. Hydrogen doping and possible formation mechanism.[1]H solid-state NMR spectra for (a–b) WT and RT-MH-0.5, (c) RT-MH (sep), (d) RT-H_2, (e) RT-Mg-H_2, (f) RT-Mg. RT-MH (sep): the sample was prepared by placing the TiO_2 and MgH_2 separately without homogeneous mixing in a ceramic boat and heated in Ar atmosphere. RT-H_2: the sample was prepared by heating in 5% H_2/Ar atmosphere. RT-Mg-H_2: the sample was prepared using magnesiothermic reduction in 5% H_2/Ar at 650 °C (as metallic Mg melts after 600 °C). RT-Mg: the sample was prepared using magnesiothermic reduction in Ar atmosphere without H_2 at 650 °C. Otherwise, the reduction temperature is set at 500 °C as mentioned in Methods. (g) A pictorial presentation of the probable process during MgH_2 reduction of TiO_2 leading to H:TiO_{2-x}.

gap of 3.21 eV, whereas the reduced materials show 2.25, 2.17 and 1.66 eV for RT-MH-0.3, 0.5 and 0.75, respectively from different patterns of Tauc plot with two slopes, unlike WT.

The valence band (VB) XPS (Fig. 3g) of the RT-MH-0.5 displays a prominent shift of peak edge towards lower binding energy compared to WT, which indicates the shifting of VB top towards Fermi level due to the formation of new energy states near to VB. Considering the band gap and VB edges, a possible band energy diagram is portrayed in Fig. 3h, which also suggests a trailing of conduction band (CB) to a decrement of the band gap. The formation of new states near CB bottom and VB top can be attributed to the Ti^{3+} and oxygen vacancies, respectively. Although the band gap and absorption are more favorable for RT-MH-0.75 compared to RT-MH-0.5, the photocatalytic activity is reverse. This behavior can be explained by accounting electron-hole recombination as one of the major controlling factors [11] measured by photoluminescence (PL) spectra, which demonstrated the lowest radiative recombination of RT-MH 0.5 (Fig. S8).

The chemical environment of 'H' in the reduced samples was studied by ^{1}H solid-state NMR (Fig. 4a–f). WT shows only one sharp peak at ~5.2 ppm which is mainly attributed to the surface hydroxyl group on anatase TiO_2 due to atmospheric water absorption. This signal arises at ~5.6 ppm for RT-MH-0.5. The observed peak shifting and broadening can be ascribed to bridging 'H' to different crystallographic planes and indicate the presence of disorder phases [46]. The reduced sample also exhibits another 6 peaks, which are absent in WT and thus, indicate major chemical environmental changes during MgH_2 reduction. These signals are indicating the presence of Ti-H and surface -OH species (Table S3). More importantly, the signal at ~0.66 ppm indicates H

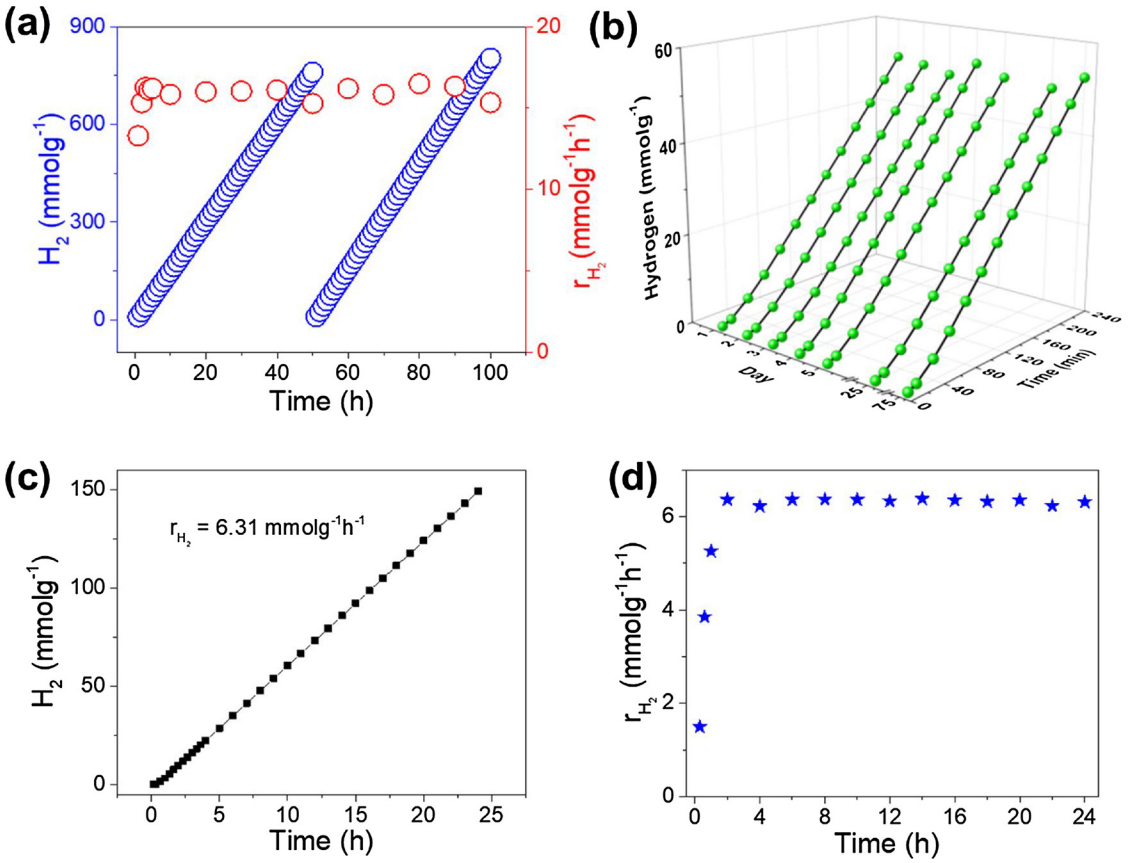

Fig. 5. Performance stability and activity in sea water. Stability study for 0.25% Pt-loaded RT-MH-0.5 for (a) continuous H_2 production and (b) long-term H_2 production in different days under simulated sunlight from methanol-water. (c) Continuous H_2 production profile from seawater and (d) rates observed in different times for H_2 production from seawater (20% methanol) by using 0.25% Pt-loaded RT-MH-0.5 under simulated sunlight (AM 1.5 G, 1 Sun).

residing at the position of oxygen vacancy, and the signal at ~0.78 suggests the dynamic, rapid exchange of 'H' between different environments provided by the disorder phases at the surface of the reduced TiO_2, which can minimize the recombination of photo-generated electrons and holes by increasing the electron transfer process [36]. Interestingly, the strong peak at ~0.66 ppm for replacement or occupation of oxygen vacancies by 'H' is not observed or only weekly observed for normal hydrogenation of TiO_2 (Fig. 4d) [46]. However, similar peaks with different intensity ratios were reported for a hydrogenated blue TiO_2 prepared from the mixture of TiO_2 and TiH_2, which showed almost double photocatalytic activity than that of pristine P25 [36]. Furthermore, the ^{1}H NMR signals observed for RT-MH-0.5 are dissimilar to the signals obtained for the samples prepared with only H_2, Mg, and Mg/H_2. In the currently developed method involving MgH_2, the 'H' replacement can be understood differently. In normal hydrogenation, H_2 reacts with surface O to form water and creates oxygen vacancies, and then 'H' can reside at the oxygen vacancies. This can result in the small amount of weakly bounded 'H' residing at reduced TiO_2 surface as observed in Fig. 4d, also reported previously [46]. In the case of MgH_2, upon decomposition at 500 °C, it will produce active "atomic" [Mg] and [H] species in a confined microenvironment, both of which can react with O to create oxygen vacancies. However, the formation free energy of MgO (-596.3 kg mol^{-1}) is much lower than that of water (gas, -228.6 kg mol^{-1}). Therefore, the formation of MgO is more favorable than water. Thus, the process can be realized as [Mg] creates the oxygen vacancies easily and then [H] may participate efficiently in the formation of Ti-H-Ti. A schematic of the probable process is presented in Fig. 4g. The formation of Ti-H and Ti-OH species has also been previously realized to improve the absorption and photocatalytic activity under visible light [36,46–51].

Furthermore, deferent experiments results clearly show that the use of MgH_2 provides more active catalyst compared to only Mg, H_2, and Mg/H_2 (Fig. S9) which suggests the synergistic effect of active [Mg] and [H] species in-situ produced from MgH_2 decomposition, which makes better photocatalyst than only hydrogenation or Mg reduction. Moreover, this high efficiency of the present photocatalyst system can be attributed to the optimum band gap and band position, enhanced absorption in visible light region, and low recombination, obtained by the synergistic effect of active [Mg] and [H] species in the controlled reducing environments.

The developed Pt/RT-MH-0.5 catalyst system exhibited outstanding performance stability as results presented in Fig. 5a and b (see Fig. S10). The study reveals the outstanding stable performance of continuous 100 h with almost the same r_{H_2} (Fig. 5a). A stable H_2 production performance is also observed for 200 h in a period of 75 days (Fig. 5b). TON (turnover number) reached around 122,656 in 100 h for RT-MH-0.5 when a minimum amount of 0.25% Pt was used (Fig. S14). The outstanding stability of RT-MH-0.5 may be accredited to the strong and optimum hydrogen doping on oxygen vacancies as discussed in Fig. 4. The excellent stability, low Pt loading, and high TON can make the developed photocatalyst system cost-effective although it still contains Pt, a high price element. The developed photocatalyst system also showed a continuous production of H_2 up to 24 h (Fig. 5c and d) with a rate of 6.31 mmolg^{-1}h^{-1} in simulated sunlight from seawater (20% methanol), the largest water source on earth. Although the activity is comparatively lower than pure water, the results are promising upon consideration of the presence of different salts and microbial components in sea water.

Figs. S11a and b represent the HR-TEM images of the photo-deposited Pt nanoparticles on RT-MH-0.5. They clearly demonstrate the

nicely distributed 2–3 nm Pt nanoparticles throughout the TiO_2 surface, which are further supported by the HR-SEM and elemental mapping. It is obvious that homogeneous distribution of small size Pt nanoparticles further improves the charge (photogenerated electron and hole) transfer process and thus overall activity. The used catalyst was characterized by HR-TEM and HR-SEM after 50 h study. Results show that the Pt nanoparticles and reduce TiO_2 are similar to the fresh catalyst (Figs. S11 and S12). No agglomeration of the Pt nanoparticles was observed, suggesting that a strong interaction between reduced H:TiO_{2-x} surface and photo-deposited Pt nanoparticles provides robust photocatalyst system. There was also no significant change (Fig. S13) in the absorbance spectra and color of RT-MH-0.5 sample prepared by MgH_2 reduction even after 3 months when stored in closed sample vial without any extra precaution in normal atmosphere.

4. Conclusions

The present work demonstrates a highly stable and efficient reduced H-doped TiO_{2-x} photocatalyst system for sunlight-induced H_2 production from methanol-water with a quantum yield of 34.6% at 340 nm, 8.66% at 400 nm, 3.95% at 420 nm, and 2.01% at 454 nm. The catalyst system can contain a minimum of 0.25% Pt nanoparticles, and a high TON of 122,656 was calculated for 100 h. The high activity is attributed to the enhanced absorption with lowered band gap and lower recombination due to optimum Ti^{3+}, oxygen vacancies, and H doping by the synergistic effect of dual reducing species ([Mg] and [H]) in a confined microenvironment from the decomposition of MgH_2. The catalyst system also showed efficient H_2 production from seawater in simulated sunlight. Moreover, the current study reveals that control modification of TiO_2 can achieve a furthermore effective visible light as well as sunlight photocatalyst system. Concerning the present requirements of sunlight-induced H_2 production photocatalyst system with high efficiency and stability, the reported work can be considered as a significant achievement with simple preparation approach.

Acknowledgements

This work was supported by Global Frontier R&D Program on Centre for Multiscale Energy System (NRF-2011-0031571) funded by the Ministry of Education, Science and Technology of Korea. Authors also would like to thank KBSIs at Busan, Seoul and Daegu and CCRF at DGIST for XPS, NMR HR-SEM, and HR-TEM measurements and Dr. Zhaohui Zhou at State Key Laboratory of Multiphase Flow in Power Engineering, at Xi'an Jiaotong University for data analysis. AS would like to thank DST, INDIA for funding through INSPIRE Faculty Scheme.

Appendix A. Supplementary data

Supplementary material related to this article can be found, in the online version, at doi:https://doi.org/10.1016/j.apcatb.2018.06.030.

References

[1] J.A. Turner, Sustainable hydrogen production, Science 305 (2004) 972–974.
[2] Y. Ma, X. Wang, Y. Jia, X. Chen, H. Han, C. Li, Titanium dioxide-based nanomaterials for photocatalytic fuel generations, Chem. Rev. 114 (2014) 9987–10043.
[3] X. Jiang, X. Fu, L. Zhang, S. Meng, S. Chen, Photocatalytic reforming of glycerol for H_2 evolution on Pt/TiO_2: fundamental understanding the effect of co-catalyst Pt and the Pt deposition route, J. Mater. Chem. A 3 (2015) 2271–2282.
[4] H. Han, C. Li, Photocatalysis in solar fuel production, Natl. Sci. Rev. 2 (2015) 145–147.
[5] M. Xing, J. Zhang, B. Qiu, B. Tian, M. Anpo, M. Che, A Brown mesoporous TiO_{2-x}/MCF composite with an extremely High quantum yield of solar energy photocatalysis for H_2 evolution, Small 11 (2015) 1920–1929.
[6] S.S. Mao, S. Shen, Hydrogen production: catalysing artificial photosynthesis, Nat. Photon. 7 (2013) 944–946.
[7] J. Liu, Y. Liu, N. Liu, Y. Han, X. Zhang, H. Huang, Y. Lifshitz, S.-T. Lee, J. Zhong, Z. Kang, Metal-free efficient photocatalyst for stable visible water splitting via a two-electron pathway, Science 347 (2015) 970–974.
[8] J. Schneider, M. Matsuoka, M. Takeuchi, J. Zhang, Y. Horiuchi, M. Anpo, D.W. Bahnemann, Understanding TiO_2 photocatalysis: mechanisms and materials, Chem. Rev. 114 (2014) 9919–9986.
[9] P. Roy, S. Berger, P. Schmuki, TiO_2 nanotubes: synthesis and applications, Angew. Chem. Int. Ed. 50 (2011) 2904–2939.
[10] D.Y.C. Leung, X.L. Fu, C.F. Wang, M. Ni, M.K.H. Leung, X.X. Wang, X.Z. Fu, Hydrogen production over titania-based photocatalysts, ChemSusChem 3 (2010) 681–694.
[11] Y.H. Hu, A highly efficient photocatalyst—hydrogenated Black TiO_2 for the photocatalytic splitting of Water, Angew. Chem. Int. Ed. 51 (2012) 12410–12412.
[12] S. Tominaka, Y. Tsujimoto, Y. Matsushita, K. Yamaura, Synthesis of nanostructured reduced titanium oxide: crystal structure transformation maintaining nanomorphology, Angew. Chem. Int. Ed. 50 (2011) 7418–7421.
[13] X. Chen, L. Liu, F. Huang, Black titanium dioxide (TiO_2) nanomaterials, Chem. Soc. Rev. 44 (2015) 1861–1885.
[14] M. Wang, B. Nie, K.-K. Yee, H. Bian, C. Lee, H.K. Lee, B. Zheng, J. Lu, L. Luo, Y.Y. Li, Low-temperature fabrication of brown TiO_2 with enhanced photocatalytic activities under visible light, Chem. Commun. 52 (2016) 2988–2991.
[15] X. Zhang, C. Wang, J. Chen, W. Zhu, A. Liao, Y. Li, J. Wang, L. Ma, Enhancement of the Field emission from the TiO_2 nanotube arrays by reducing in a $NaBH_4$ solution, ACS Appl. Mater. Interfaces 6 (2014) 20625–20633.
[16] H. Tan, Z. Zhao, M. Niu, C. Mao, D. Cao, D. Cheng, P. Feng, Z. Sun, A facile and versatile method for preparation of colored TiO_2 with enhanced solar-driven photocatalytic activity, Nanoscale 6 (2014) 10216–10223.
[17] X. Liu, G. Zhu, X. Wang, X. Yuan, T. Lin, F. Huang, Progress in black titania: a new material for advanced photocatalysis, Adv. Energy Mater. 6 (2016) 1600452.
[18] K. Zhang, L. Wang, J.K. Kim, M. Ma, G. Veerappan, C.-L. Lee, K.-j. Kong, H. Lee, J.H. Park, An order/disorder/water junction system for highly efficient co-catalyst-free photocatalytic hydrogen generation, Energy Environ. Sci. 9 (2016) 499–503.
[19] Z. Wang, C. Yang, T. Lin, H. Yin, P. Chen, D. Wan, F. Xu, F. Huang, J. Lin, X. Xie, M. Jiang, Visible-light photocatalytic, solar thermal and photoelectrochemical properties of aluminium-reduced black titania, Energy Environ. Sci. 6 (2013) 3007–3014.
[20] Y. Wang, J. Cai, M. Wu, H. Zhang, M. Meng, Y. Tian, T. Ding, J. Gong, Z. Jiang, X. Li, Hydrogenated cage-like titania hollow spherical photocatalysts for hydrogen evolution under simulated solar light irradiation, ACS Appl. Mater. Interfaces 8 (2016) 23006–23014.
[21] G. Zhu, H. Yin, C. Yang, H. Cui, Z. Wang, J. Xu, T. Lin, F. Huang, Black titania for superior photocatalytic hydrogen production and photoelectrochemical water splitting, ChemCatChem 7 (2015) 2614–2619.
[22] G. Li, J. Li, G. Li, G. Jiang, N and Ti^{3+} co-doped 3D anatase TiO_2 superstructures composed of ultrathin nanosheets with enhanced visible light photocatalytic activity, J. Mater. Chem. A 3 (2015) 22073–22080.
[23] N. Liu, V. Häublein, X. Zhou, U. Venkatesan, M. Hartmann, M. Mackovic, T. Nakajima, E. Spiecker, A. Osvet, L. Frey, P. Schmuki, 'Black' TiO_2 nanotubes formed by high energy proton implantation show noble-metal-co-catalyst free photocatalytic H_2-evolution, Nano Lett. 15 (2015) 6815–6820.
[24] Y. Xu, C. Zhang, L. Zhang, X. Zhang, H. Yao, J. Shi, Pd-Catalyzed instant hydrogenation of TiO_2 with enhanced photocatalytic performance, Energy Environ. Sci. 9 (2016) 2410–2417.
[25] K. Zhang, J.H. Park, Surface localization of defects in Black TiO2: enhancing photoactivity or reactivity, J. Phys. Chem. Lett. 8 (2017) 199–207.
[26] A. Saha, A. Sinhamahapatra, T.H. Kang, S.C. Ghosh, J.S. Yu, A.B. Panda, Hydrogenated MoS_2 QD-TiO_2 heterojunction mediated efficient solar hydrogen production, Nanoscale 9 (2017) 17029–17036.
[27] A. Razzaq, A. Sinhamahapatra, T.-H. Kang, C.A. Grimes, J.-S. Yu, S.-I. In, Efficient Solar Light Photoreduction of CO_2 to Hydrocarbon Fuels via Magnesiothermally Reduced TiO_2 Photocatalyst, Appl. Catal. B Environ. (2017).
[28] G. Wang, H. Wang, Y. Ling, Y. Tang, X. Yang, R.C. Fitzmorris, C. Wang, J.Z. Zhang, Y. Li, Hydrogen-treated TiO2 nanowire arrays for photoelectrochemical water splitting, Nano Lett. 11 (2011) 3026–3033.
[29] S. Tominaka, Topotactic reduction yielding black titanium oxide nanostructures as metallic electronic conductors, Inorg. Chem. 51 (2012) 10136–10140.
[30] Y. Shan, Y. Yang, Y. Cao, H. Yin, N.V. Long, Z. Huang, Hydrogenated black TiO_2 nanowires decorated with Ag nanoparticles as sensitive and reusable surface-enhanced Raman scattering substrates, RSC Adv. 5 (2015) 34737–34743.
[31] Q. Kang, J. Cao, Y. Zhang, L. Liu, H. Xu, J. Ye, Reduced TiO_2 nanotube arrays for photoelectrochemical water splitting, J. Mater. Chem. A 1 (2013) 5766–5774.
[32] J. Tian, X. Hu, H. Yang, Y. Zhou, H. Cui, H. Liu, High yield production of reduced TiO2 with enhanced photocatalytic activity, Appl. Surf. Sci. 360 (Part B) (2016) 738–743.
[33] L. Liu, Y. Jiang, H. Zhao, J. Chen, J. Cheng, K. Yang, Y. Li, Engineering coexposed {001} and {101} facets in oxygen-deficient TiO2 nanocrystals for enhanced CO2 photoreduction under visible light, ACS Catal. 6 (2016) 1097–1108.
[34] H. Li, J. Chen, Z. Xia, J. Xing, Microwave-assisted preparation of self-doped TiO_2 nanotube arrays for enhanced photoelectrochemical water splitting, J. Mater. Chem. A 3 (2015) 699–705.
[35] X. Xin, T. Xu, J. Yin, L. Wang, C. Wang, Management on the location and concentration of Ti3+ in anatase TiO2 for defects-induced visible-light photocatalysis, Appl. Catal. B Environ. 176–177 (2015) 354–362.
[36] G. Zhu, Y. Shan, T. Lin, W. Zhao, J. Xu, Z. Tian, H. Zhang, Z. Chong, F.Q. Huang, Hydrogenated Blue titania with High solar absorption and greatly improved photocatalysis, Nanoscale 8 (2016) 4705–4712.
[37] A. Sinhamahapatra, J.-P. Jeon, J.-S. Yu, A new approach to prepare highly active and stable black titania for visible light-assisted hydrogen production, Energy Environ. Sci. 8 (2015) 3539–3544.

[38] A. Sinhamahapatra, J.P. Jeon, J. Kang, B. Han, J.S. Yu, Oxygen-deficient zirconia (ZrO_{2-x}): a New material for solar light absorption, Sci. Rep.-UK 6 (2016) 27218.
[39] A. Jain, S. Agarwal, S. Kumar, S. Yamaguchi, H. Miyaoka, Y. Kojima, T. Ichikawa, How does TiF4 affect the decomposition of MgH_2 and its complex variants?—An XPS investigation, J. Mater. Chem. A 5 (2017) 15543–15551.
[40] T. Xia, X. Chen, Revealing the structural properties of hydrogenated black TiO_2 nanocrystals, J. Mater. Chem. A 1 (2013) 2983–2989.
[41] Z. Wei-Dong, W. Cheng-Wei, C. Jian-Biao, L. Dong-Sheng, Z. Feng, Z. Hao-Li, Enhanced field emission from hydrogenated TiO_2 nanotube arrays, Nanotechnology 23 (2012) 455204.
[42] X. Yu, B. Kim, Y.K. Kim, Highly enhanced photoactivity of anatase TiO2 nanocrystals by controlled hydrogenation-induced surface defects, ACS Catal. 3 (2013) 2479–2486.
[43] G. Zhu, T. Lin, X. Lu, W. Zhao, C. Yang, Z. Wang, H. Yin, Z. Liu, F. Huang, J. Lin, Black brookite titania with high solar absorption and excellent photocatalytic performance, J. Mater. Chem. A 1 (2013) 9650–9653.
[44] C. Zhen, L. Wang, L. Liu, G. Liu, G.Q. Lu, H.-M. Cheng, Nonstoichiometric rutile TiO_2 photoelectrodes for improved photoelectrochemical water splitting, Chem. Commun. 49 (2013) 6191–6193.
[45] T. Xia, C. Zhang, N.A. Oyler, X. Chen, Hydrogenated TiO2 nanocrystals: a novel microwave absorbing material, Adv. Mater. 25 (2013) 6905–6910.
[46] X. Chen, L. Liu, Z. Liu, M.A. Marcus, W.-C. Wang, N.A. Oyler, M.E. Grass, B. Mao, P.-A. Glans, P.Y. Yu, J. Guo, S.S. Mao, Properties of disorder-engineered Black titanium dioxide nanoparticles through hydrogenation, Sci. Rep. 3 (2013) 1510.
[47] P. Jonsen, Identification of different hydrogen-reduced titania crystallographic forms by ^1H NMR spectroscopy, Catal. Lett. 2 (1989) 345–349.
[48] N. Liu, C. Schneider, D. Freitag, M. Hartmann, U. Venkatesan, J. Muller, E. Spiecker, P. Schmuki, Black TiO_2 nanotubes: cocatalyst-Free Open-circuit hydrogen generation, Nano Lett. 14 (2014) 3309–3313.
[49] T.D. Nguyen-Phan, S. Luo, Z.Y. Liu, A.D. Gamalski, J. Tao, W.Q. Xu, E.A. Stach, D.E. Polyansky, S.D. Senanayake, E. Fujita, J.A. Rodriguez, Striving toward noble-metal-Free photocatalytic Water splitting: the hydrogenated-graphene-TiO_2 prototype, Chem. Mater. 27 (2015) 6282–6296.
[50] W. Wei, N. Yaru, L. Chunhua, X. Zhongzi, Hydrogenation of TiO_2 nanosheets with exposed {001} facets for enhanced photocatalytc activity, RSC Adv. 2 (2012) 8286–8288.
[51] C. Yang, Z. Wang, T. Lin, H. Yin, X. Lü, D. Wan, T. Xu, C. Zheng, J. Lin, F. Huang, X. Xie, M. Jiang, Core-shell “Black” Rutile titania as excellent catalyst for hydrogen production enhanced by sulfur doping, J. Am. Chem. Soc. 135 (2013) 17831–17838.